Highlights

Vertical Structure of Flows on a Shallow Reef Flat: A Coral Reef Surf Zone

Stephen G. Monismith,Samantha A. Maticka,Justin S. Rogers,Ben Hefner,C. Brock Woodson

- Vertical flow structure for wave-driven flow on a shallow coral reef resembles surf-zone
- Shear in cross-reef flow can be modeled using a wave-based eddy viscosity
- The depth-averaged mean flow on the reef flat is not predicted a priori

Vertical Structure of Flows on a Shallow Reef Flat: A Coral Reef Surf Zone

Stephen G. Monismith[a,*], Samantha A. Maticka[a,b], Justin S. Rogers[a], Ben Hefner[c] and C. Brock Woodson[c]

[a]Bob and Norma Street Environmental Fluid Mechanics Laboratory, Stanford University, Stanford, California, 94305-4020, USA
[b]GEOSCIENCES-Montpellier, Université Montpellier, CNRS, Montpellier, 34095 France
[c]College of Engineering, University of Georgia, Athens, Georgia, 30602, USA

ARTICLE INFO

Keywords:
coral reef
waves
surfzone
turbulence

ABSTRACT

We present a 1D model of the vertical structure of wave-driven flows on a shallow coral reef and compare that model to observations made on the reef flat on Ofu, American Samoa. This model is based on longstanding approaches to modeling flow structure in beach surf zones including the averaged effects of breaking and broken surface waves. Waves enter the model through an imbalance between the radiation stress and barotropic pressure gradients that exists below the troughs of the waves, which is offset by turbulent shear stress gradients. Assuming that the depth varying eddy viscosity takes the form found in open channel flows, i.e., a parabola, the horizontal momentum equation can be integrated twice with respect to height to derive the distribution with height of the velocity. The resulting theory is compared to observations made on a reef flat located on Ofu, American Samoa. Using a velocity scale in the eddy viscosity model that is proportional to the rms wave velocity, modeled profiles match observations reasonably well (average skill= 0.66), although there is some ambiguity introduced because matching observations and theory requires the addition of a correction that is found to depend on the square of the rms wave height.

1. Introduction

Waves and wave-driven flows in beach surf zones have received considerable attention (e.g. Battjes (1988)) because of their importance to surf zone sediment transport and thus to beach evolution (Roelvink and Reniers, 2012; Raubenheimer et al., 1995), as well as to cross-shore exchange of contaminants and larvae between the surf zone and the inner shelf offshore (Grant et al., 2005; Morgan et al., 2018)). The transformation of incident waves due to shoaling and breaking can be predicted with some accuracy using models that represent the phase-averaged properties of breaking (e.g.,Thornton and Guza (1983); Raubenheimer et al. (1996); Apotsos et al. (2007, 2008)).

Similar models have been employed to look at wave transformation and breaking on coral reefs, although reflecting the intrinsic rugosity of coral reefs, bottom roughness can have much larger effect on wave height on reefs than on beaches (Lowe et al., 2005; Becker et al., 2014; Monismith et al., 2015). Moreover, while the model proposed by Thornton and Guza (1983) for wave breaking on mildly sloping beaches provides a reasonably accurate model of dissipation due to breaking on beaches, wave-breaking on coral reefs, which typically have steep faces, is more complex (Yao et al., 2012; Monismith et al., 2013; Becker et al., 2014; Buckley et al., 2016), such that the applicability of models like that of Thornton and Guza (1983) may be questionable.

The theory of wave-averaged (hereafter "mean") flows on beaches is largely based on the pioneering analysis of Longuet-Higgins and Stewart (1962), who showed how wave shoaling and breaking produce net forces in the surfzone that can drive alongshore flows and produce mean setups and set downs of the free surface (e.g., Ruessink et al. (2001)). Moreover, as first shown by Svendsen (1984b), because forces exerted by the waves on the mean flow vary with height, they produce a vertically sheared velocity profile with offshore flow, the undertow, over much of the water column (Svendsen, 1984b; Reniers et al., 2004).

In this paper we present an application of Svendsen's theory to the description of the vertical structure of cross-reef flows measured on a shallow reef flat on the south shore of Ofu, American Samoa. The model we present looks very much like that which Reniers et al. (2004) used to describe mean Eulerian flows on the beach at Sandy Duck, with one important difference between the two: For the beach flow, the depth integrated Lagrangian mean flow (Longuet-Higgins, 1969) is zero, whereas there is net transport, both onshore and offshore, on the reef flat. Detailed descriptions of the waves and flows on the reef can be found in Maticka et al. (2022), so only a brief description will be given in section 3. As we will show, using an eddy viscosity proportional to local wave velocities to model turbulent stresses, Svendsen's theory provides a good prediction of the vertical structure of the mean Eulerian flows on the Ofu reef flat, including showing the existence of an undertow at times when the flow is relatively deep, and purely onshore flows near low tide.

2. Theory

The fundamental basis for the analysis that follows is the widely used wave-averaged, depth-integrated momentum equation with advective accelerations assumed to be small. (Mei et al., 1989; Ruessink et al., 2001; Apotsos et al.,

*Corresponding author
monismith@stanford.edu (S.G. Monismith)
ORCID(s):

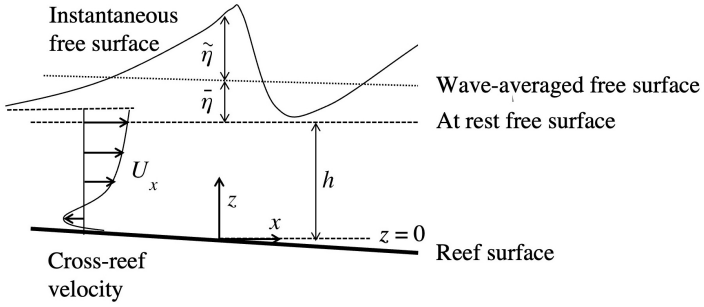

Figure 1: Definition sketch for model. Note that in this sketch the reef flat is shown as becoming deeper in the shoreward direction as is observed on Ofu.

2008; Becker et al., 2014), here written for the cross-shore direction x pointing towards land (Fig. 1):

$$gh_i\frac{d\overline{\eta}}{dx} = -\frac{1}{\rho}\frac{dS_{xx}}{dx} - \frac{1}{\rho}\frac{dR}{dx} - \frac{\tau_b}{\rho} \tag{1}$$

In this equation $\overline{\eta}$ is the wave-averaged deviation of the free surface from equilibrium (positive up), S_{xx}, is the radiation stress, R is the stress exerted by the surface roller, and τ_b is the mean bottom stress (Apotsos et al., 2008). The wave-averaged depth $h_i = h + \overline{\eta}$ is defined as the sum of the spatially varying water depth when the water surface is flat, $h(x)$, and the variation $\overline{\eta}(x,t)$ due to waves and tides (Maticka et al., 2022). We can write any variable in the form $f = \overline{f} + \tilde{f}$, where $\overline{f}$ is the wave-averaged value of f and $\tilde{f}$ is the deviation of f from that average. We assume that the averaging period is long enough to filter out both sea swell and infragravity waves.

In shallow water,

$$S_{xx} = (3/2)\rho g\overline{\tilde{\eta}^2} \tag{2}$$

where $\tilde{\eta}$ is the instantaneous value of the deviation of the free surface from its mean position due to the waves. The surface roller stress is parameterized as Svendsen (1984a)

$$R = \rho\frac{A_r C}{T} \tag{3}$$

where A_r is the area of the roller and, C is the phase speed and T is the wave period. A_r is usually computed using an evolution equation for which the rate of dissipation due to breaking is a source term and for which there is a roller dissipation term that acts as a sink (Reniers et al., 2004). Svendsen (1984b) assumed that in terms of wave height H, $A_r = 0.9H^2 \approx 3.6\overline{\tilde{\eta}^2}$, whereas surf zone LIDAR measurements reported by Martins et al. (2018) were well described by $A_r = 1.1\overline{\tilde{\eta}^2}$. Using this latter relation for A_r, R was estimated to be ca. 2 % of S_{xx} for the Ofu reef flat, and so was neglected in the analysis of our Ofu observations. Nonetheless, R is retained in the equations below for the sake of completeness.

The local momentum equation valid below the wave trough (Svendsen's eq. 4.1) reads

$$\frac{\partial}{\partial z}\left(\nu_t\frac{\partial\overline{U}_x}{\partial z}\right) = \frac{\partial\overline{\tilde{U}_x^2}}{\partial x} + g\frac{\partial\overline{\eta}}{\partial x} \tag{4}$$

In eq.4, z is the vertical coordinate measured upwards from the (local) reef surface ($z = 0$), $\overline{U_x}$ is the mean Eulerian cross-reef velocity, and $\tilde{U}_x$ is the cross reef wave velocity. Thus, using eq. 1, eq.4 becomes

$$\frac{\partial}{\partial z}\left(\nu_t\frac{\partial\overline{U_x}}{\partial z}\right) = \frac{\partial\overline{\tilde{U}_x^2}}{\partial x} - \frac{1}{\rho h_i}\frac{\partial S_{xx}}{\partial x} - \frac{1}{\rho h_i}\frac{\partial R}{\partial x} - \frac{\tau_b}{\rho h_i} \tag{5}$$

To the extent that an eddy viscosity model of turbulent stresses in the presence of waves is appropriate and in the limit where the waves are long, eq. 4 is exact. However, it only applies to that part of the water column that is below the wave troughs for the entire averaging period, h_s. For the Ofu reef flat, on average, h_s was greater than $0.9h_i$, and was less than $0.8h_i$ for less than 5% of the measurement period. Linearization might be required to compute $\tilde{U}_x$ and S_{xx}, although, as noted by Monismith et al. (2013), in the long wave limit these can be computed from data without assuming that the waves are sinusoidal. However, it should be recognized that values of S_{xx} (in particular) based on linear theory may be underestimates of the actual radiation stress (Stive and Wind, 1982; Buckley et al., 2015) and that in contrast to eq. 6 below, $\tilde{U}_x$ may vary with depth (Stive and Wind, 1982; Govender et al., 2011).

The shallow water limit of S_{xx} is given by 2 and

$$\overline{\tilde{U}_x^2} = \frac{g\overline{\tilde{\eta}^2}}{h_i} \tag{6}$$

so that

$$\frac{\partial}{\partial z}\left(\nu_t\frac{\partial\overline{U_x}}{\partial z}\right) = -\frac{g}{2h_i}\frac{\partial\overline{\tilde{\eta}^2}}{\partial x} - \frac{\partial h_i}{\partial x}\frac{g\overline{\tilde{\eta}^2}}{h_i^2} - \frac{1}{\rho h_i}\frac{\partial R}{\partial x} - \frac{\tau_b}{\rho h_i}$$
$$= a(x) - \frac{\tau_b}{\rho h_i}$$

(7)

Here $a(x)$ represents the first three terms on the right hand side of eq. 7, or equivalently, the first two terms on the right hand side of eq. 5. If $\frac{\partial h_i}{\partial x} \approx 0$, eq. 2 and eq. 7 imply that in shallow water, 2/3 of the wave forcing other than the roller stress appears to act above the troughs of the waves.

Including the bottom boundary condition on the stress, integration twice with respect to z gives:

$$\overline{U_x} = \int_{z_b}^{z} \frac{a(x)\,\xi + \left(\tau_b/\rho\right)\left(1 - \xi/h_i\right)}{\nu_t(\xi)} d\xi + c(x) \quad (8)$$

where z_b is the height near the bottom where the turbulent stress is equal to τ_b. The bottom kinematic boundary condition gives:

$$\overline{U_x}(z_b) = U_0 \Rightarrow c(x) = U_0 \quad (9)$$

with U_0 equal to the velocity near the bottom. This will be specified later.

A common model for eddy viscosity in shallow flows is the parabolic distribution (Reniers et al., 2004):

$$\nu_t = \kappa u_* z \left(1 - z/h_i\right) \quad (10)$$

where u_* is the bottom friction velocity, although in the present case, this may not be the correct velocity scale. As an alternative, we re-write this as

$$\nu_t = \nu_0 \left(z/h_i\right)\left(1 - z/h_i\right) \quad (11)$$

where ν_0 is expected to be a function of the strength of turbulence produced by wave breaking and by bottom boundary layer turbulence also associated with the waves. Thus, eq. 8 becomes

$$\begin{aligned}\overline{U_x}(z) &= -\frac{h_i^2 a}{\nu_0} \int_{\frac{z_b}{h_i}}^{\sigma} \frac{1}{(1-\zeta)} d\zeta \\ &\quad + \left(\frac{\tau_b h_i}{\rho \nu_0}\right) \int_{\frac{z_b}{h_i}}^{\sigma} \frac{d\zeta}{\zeta} + U_0 \\ &= A \log\left(\frac{h_i - z}{h_i - z_b}\right) + B \log\left(\frac{z}{z_b}\right) + U_0\end{aligned} \quad (12)$$

where $\sigma = z/h_i$. Note that z_b could be chosen to be roughness length z_0, as is customary for turbulent channel flows. The two constants are

$$A = \frac{h_i a}{\nu_0} \quad B = \frac{\tau_b h_i}{\rho \nu_0} \quad (13)$$

Not surprisingly, eq. 12 appears to be identical to eq. B13 in Reniers et al. (2004), a likely consequence of the parabolic eddy viscosity and depth-invariant forcing used in both their and our models. One feature that emerges from eqs. 12 and 13 is that while the shore-ward decrease in wave height always produces onshore flows (the first term on the rhs of eq. 12 is always positive), the term involving the bottom stress, which can have either sign, can lead to flows either towards or away from shore. Thus, for an undertow to exist, the bottom stress must be negative, i.e., directed offshore, a condition that requires the velocity to be offshore (negative) near the bottom. The total shore-normal flow is:

$$q_T = q_E + q_W + q_R = \int_0^{h_i} \overline{U_x} dz + \overline{\tilde{U}_x \tilde{\eta}} + A_r/T \quad (14)$$

where q_E is the mean Eulerian transport, q_W is the wave transport and q_R is the roller transport. Given that the second two terms on the rhs of 14, are onshore, q_E must be directed offshore on beaches, so that $q_T = 0$. For reef flats, this isn't necessarily the case, since the total flow can be either onshore or offshore, depending on tides and wave forcing, and possibly location on the reef (Maticka et al., 2022).

The problem as posed requires two boundary conditions. One of these, the bottom stress condition was used in the integration that gives eq.12. For the second condition, rather than impose a stress at the surface (a possible second condition), we choose to specify U_0. Hence, there are two parameters, ν_0 and U_0 to be determined by matching theory to observations. In the absence of some form of turbulence closure that explicitly accounts for wave breaking and wave turbulence interactions, a simpler approach is to assume that ν_0 is the product of suitable velocity and length scales, as did Reniers et al. (2004),

$$\nu_0 = \alpha\, U_{rms} h_i \quad (15)$$

where $U_{rms} = \sqrt{\tilde{U}_x^2}$ is the rms wave-induced velocity Reniers et al. (2004). For U_0, there are several possibilities. Svendsen (1984) suggests that U_0 could be estimated from bottom boundary layer streaming (as in Longuet-Higgins (2005)), an approach followed by Reniers et al. (2004) that may be appropriate on beaches. Alternatively, as in turbulent channel flows, U_0 could be set equal to 0 with z_b chosen to be the roughness height z_0 (Pope, 2000). A third possibility is that U_0 can be determined by requiring that the mean Eulerian transport calculated by the model is the same as that observed. Given the limitations of our data, we chose this last approach to evaluate U_0. This choice will be discussed further below.

Lastly, the eddy viscosity could be assumed to be constant rather than varying with height (Svendsen, 1984b). In this case, eq. 12 becomes:

$$\begin{aligned}\overline{U_x} &= -\frac{h_i}{2\nu_0}\frac{\partial F}{\partial x}\left\{\left(\frac{z}{h_i}\right)^2 - \left(\frac{z_b}{h_i}\right)^2\right\} \\ &+ \frac{\tau_b h_i}{\rho \nu_0}\left\{\left(\frac{z}{h_i}\right) - \left(\frac{z_b}{h_i}\right) - \frac{1}{2}\left(\frac{z}{h_i}\right)^2 + \frac{1}{2}\left(\frac{z_b}{h_i}\right)^2\right\} + U_0\end{aligned} \quad (16)$$

As we will briefly discuss below, the model with variable ν_t (eq.12) showed only slightly better predictive skill than did the model with constant ν_t.

3. Observations

All of the velocity measurements to which we will apply the model developed above were made on the reef flat of pool 400, located on the south shore of Ofu, American Samoa between March 14th and March 19th, although a larger suite of instruments was deployed at the site (including on the fore-reef), from March 10 to March 28, 2017 (Rogers et al., 2018; Maticka, 2019; Maticka et al., 2022). This barrier reef system has a steep forereef (ca. 15% slope), a shallow (0.5 to 1.5 m deep) reef flat that is about 100 m wide and next to the shore, a ca. 2m deep lagoon (Oliver and Palumbi, 2009). The reef flat is a low-relief hard surface with mostly sparse small branching coral colonies (Maticka, 2019). There are several narrow channels cut through the reef flat, connecting the lagoon to the offshore ocean.

As discussed in Rogers et al. (2018) mean flows through the Ofu reef system, primarily onshore over the reef flat, alongshore in the lagoon and back offshore through the channels (Monismith, 2014), are driven by wave breaking on the forereef (e.g. Symonds et al. (1995)). After breaking, the waves propagate as turbulent bores across the reef flat (Maticka et al., 2022). Both the mean flow and the waves vary with the 1 m tidal variation in depth on the reef flat.

The measurements we will compare to field observations include velocity profiles measured at station D-4 in the middle of the reef flat using an RDI vADCP (Hefner et al., 2019; Maticka et al., 2022). The vADCP recorded data at 3 sec intervals in 3 cm bins starting 0.11 mab and extending through approximately 90% of the local depth. To compute wave-averaged velocities, raw vADCP velocities were averaged over non-overlapping 1 hour segments. This averaging removes both sea swell and infragravity wave bands variance. RBR solo pressure loggers sampling at 2 Hz were deployed at a variety of stations on the fore-reef, reef flat, and in the lagoon (Maticka, 2019). These data were processed to compute mean free surface elevation gradients and free surface height variances and thus radiation stresses and estimated wave velocities (Maticka et al., 2022). The locations of the pressure sensors used to derive S_{xx} etc, along with that of the vADCP are shown in Fig. 2.

Because the pressure sensor at D-4 did not record data, wave properties at D-4 were estimated by linear interpolation of wave properties at D-5 and D-3. Likewise, gradients of S_{xx} and $\overline{\tilde{U}_x^2}$ (c.f. eq.5) at D-4 were computed as the difference between properties at D-3 and D-5, e.g., $\partial S_{xx}/\partial x = \Delta S_{xx}/\Delta x$. The bottom shear stress, τ_b was computed from the overall momentum balance (eq. 1) as the difference between $\frac{1}{h_i}\frac{\partial S_{xx}}{\partial x}$ and $\rho g \frac{\partial \overline{\eta}}{\partial x}$ (see also Sous et al. (2022)). Given that the dissipation rate due to breaking was much smaller than that due to bottom friction, the roller force (eq. 3) was assumed to be negligible. Quantification of the fidelity of the various aspects of models used to describe flows on the Ofu reef use the coefficient of determination (r^2) and the Willmott skill score, hereinafter referred to as "skill" (Willmott, 1981) .

Conditions existing during the 5 days for which the vADCP at D-4 recorded velocities are shown in Fig.3. While the significant wave height at FR05 varied between 0.5 m and 1.2 m for the period shown in Fig.3, the wave height at D-4 primarily varied with water depth, reflecting depth-limited breaking at the ocean-ward edge of the reef flat (Maticka et al., 2022). At the beginning of this period, the tidally varying flow over the reef flat was directed onshore whereas the last two days included periods in which the flow at D-4 was directed offshore. Onshore flows in the first part of this period are what is expected for wave-driven circulation on the Ofu reef flat whereas, net offshore flows seen later on are symptomatic of rip-current like behavior observed on the Ofu reef, i.e., locally isolated currents directed opposite to the incoming waves. As discussed by Lindhart et al. (2021), this behavior is symptomatic of "closed" reefs, i.e., reefs that behave like beaches.

For most of the 5 days shown in Fig.3, the primary force balance is between the onshore directed forcing of the radiation stress gradient and offshore directed pressure gradient, i.e., $-dS_{xx}/dx \approx \rho g h_i \overline{\eta}/dx$. The difference between these two terms is made up by the bottom stress, which acts in the onshore direction at times and in the offshore direction at other times. Assuming that $\nu_t > 0$, when $\tau_b > 0$, $\partial \overline{U}_x/\partial z > 0$, and so near-bed flows are onshore, whereas when $\tau_b < 0$, $\partial \overline{U}_x/\partial z < 0$, and so $\overline{U}_x < 0$ near the bed. As seen in Fig.3, times when $\overline{U}_x < 0$ are also times when $\tau_b < 0$; indeed, r^2 for the relation $\overline{U}_x\ (z = 0.1\ \text{mab}) = 0.12\ \tau_b$ is 0.98. Thus when $\tau_b < 0$ there is an undertow, at least near the bed. However, in general, the range of depths for which $\overline{U}_x < 0$ depends on the relative sizes of the two forcing terms, A and B, in eq. 13.

4. Application of the Vertical Structure Model

In this section we will apply the model presented in section 2 to the Ofu reef flat observations. To do so requires specifying the constant α appearing in eq. 15, the reference height z_b and finding U_0. By trial and error we found that $\alpha \simeq 0.07$ produced velocity profiles that best matched observed vertical shears and produced the highest median value of skill (0.66) for the entire set of 127 profiles. U_0 was chosen for each profile such that model depth-averaged velocity equaled the measured depth-average velocity. This was the least satisfactory aspect of the model application and will be discussed further below.

A comparison of theory and observations for one day early in the period for which the vADCP was working are shown in Fig. 4. During this period, the strongest onshore flows were observed and r^2 values were generally quite high. Nonetheless, there are several examples of undertow profiles, notably near high water, in this set of velocity profiles. One systematic difference is that the observed velocities are generally higher near the water surface, i.e., for

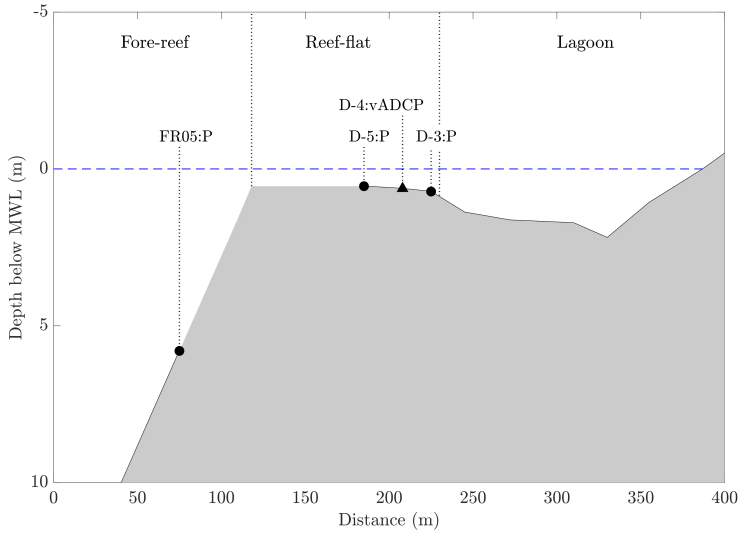

Figure 2: Locations of the instruments deployed on the Ofu reef in March 2017. Stations marked with a P denote locations where pressure sensors were deployed. An estimate of the bathymetry at mean water level is also shown.

$z > h_i - H_s/2$, where H_s is the significant wave height, than the model predicts. This may reflects a shore-ward (positive) biasing of the near-surface observations because above the wave troughs, the vADCP should preferentially measure shore-ward wave velocities. The strongly sheared near-surface region may also be due to the depth-variable effects of the surface roller, which can act like an shear stress imposed at the free surface Svendsen (1984b); Reniers et al. (2004). Svendsen (1984b) suggested that ν_t should decay exponentially from the surface under broken waves. However, this would produce velocity profiles that are less sheared near the surface than are profiles predicted with the parabolic distribution of ν_t. Thus, while intuitively appealing, the exponential model for ν_t is not likely to be an accurate model of turbulent mixing on the reef flat.

A similar comparison for a day at the end of the period of vADCP operation shows profiles for times when there is significant undertow (e.g. Fig. 5 b, c, h, and i), mostly at high tide, as well as nearly uni-directional onshore flows (e.g. Fig. 5 a, f, and m), mostly at low tide. Notably the model fidelity is lower for the profiles with strong undertow (e.g., Fig. 5 j) than for profiles with strong onshore flows (e.g., Fig. 5 a). As with the first set of profiles, near-surface velocities are systematically higher than theory predicts.

The Wilmott skill score and r^2 were calculated separately for each velocity profile. The performance of the model (skill and r^2) is best for onshore flows and near high water, both calculated only for $z < h_i - H_s/2$, i.e., below wave troughs (Fig. 6a,b). Overall the median values for the skill and r^2 are respectively 0.66 ± 0.02 and 0.75 ± 0.03. In general, the lowest (and most variable) values of both parameters are found when the depth-averaged mean Eulerian velocity, $< \overline{U}_x > \approx 0$. However, the particularly low values of r^2 also result from there being little velocity variability in the water column, as seen in Fig. 5j where much of the variability is due to instrument noise.

Following Reniers et al. (2004), both the Wilmott skill score and r^2 were also calculated for the time series at each depth where there were at least 10 measured velocities (Fig. 6c). Because of both waves and tides, the fraction of time for which the vADCP measurement volume was in the water and hence could measure velocities decreased with height above the bed, such that above $z = 0.74$ mab, good mean velocities were obtained less than 10% of the time. As seen in Fig. 6c, both model performance metrics were better higher in the water column than near the bottom. It is possible that this reflects the effects of local reef topography since individual roughness elements (sparse corals) on the reef were O(10) cm high. It may also indicate that the effects of the wave boundary layer on the mean flow (c.f. Longuet-Higgins (2005)), notably the wave stresses, net momentum fluxes due to the horizontal and vertical wave velocities being out of quadrature (Nielsen, 1992) are not properly represented by the eddy viscosity model. Finally, a scatter plot of predicted and observed velocities less their depth-averaged means (Fig. 6d) makes clear that the model described above provides reasonably accurate predictions of vertically variable velocities on the reef flat. I.e., individual observed velocities are $1.015 \times$ their respective predicted velocities with $r^2 = 0.93$, and the overall model skill (computed pointwise) was 0.87.

The skill values found for modelling the Ofu reef flat flows are comparable to the values reported by Reniers et al. (2004). The considerable range in model skill seen in Reniers et al. (2004) depended on whether the model coefficients were chosen for each profile so as to best fit the data or were calibrated so as to use one set of parameters for the entire data, as we have done here. However, one difference between the two models is that the eddy viscosity

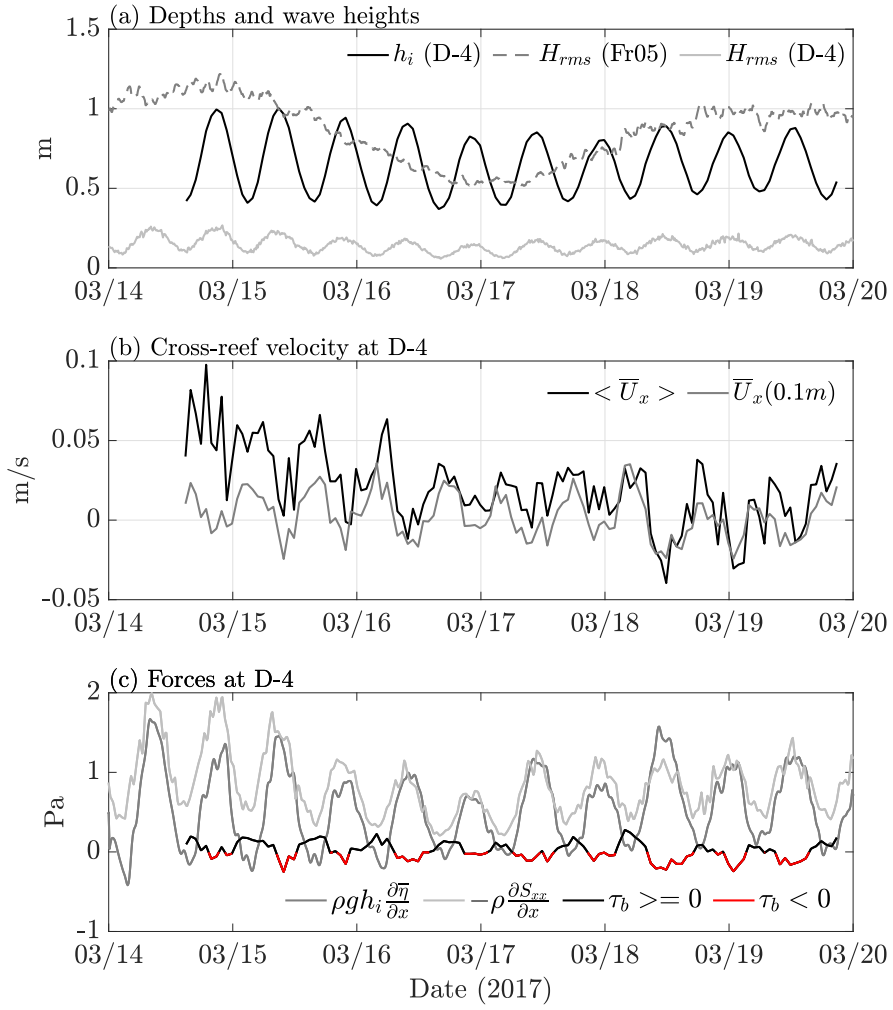

Figure 3: Forcing and flows on the Ofu reef flat: (a) tidal depth and rms wave height variations at D-4 and rms wave height variations at FR5; (b) Depth-averaged (<>) and near bottom ($z = 0.1$ mab) values of $\overline{U}_x$ at D-4; (c) Forces acting on the water column at D-4. Periods of time when $\tau_b < 0$ are noted on this figure.

model of Reniers et al. (2004) combines the effects of the waves, albeit parameterized in terms of the computed roller dissipation and H_{rms}, and the mean longshore flow, whereas our model is based solely on the local wave velocity. The constant $\alpha = 0.07$ in eq. 15, is approximately 40% of what would be computed assuming that the relevant turbulent velocity scale is based on the bottom friction associated with the waves, $u_{*w} = \sqrt{f_w} U_{rms}$, and that $\nu_0 = \kappa u_{*w} h_i$, where $\kappa = 0.4$ is the von Kármán constant. One difference between the skill profile shown in Fig. 6c and values reported by Reniers et al. (2004) is that our values of skill are best above the bottom whereas those of Reniers et al. (2004) are best near the bottom and are significantly lower near the water surface.

One further test of the model is to compare the bottom stress inferred from the overall momentum balance to the bottom stress that would be computed using the modeled eddy viscosity and the observed near bottom shear, computed by differencing the velocities at $z = 0.1$ mab and 0.16 mab (Fig. 7). In this case, it appears that the bottom stress would be best predicted with $\alpha = 0.05$ rather than $\alpha = 0.07$. This again suggests that that the eddy viscosity model for the bottom stress may need correction in some fashion to properly account for the effects of the wave effects near the bottom.

Nearly identical values of skill and r^2 were obtained using the constant eddy viscosity model as were seen with the parabolic viscosity model, albeit with $\alpha = 0.012$, rather than $\alpha = 0.018$, the value that would represent the average of the parabolic viscosity distribution that produced the best match to observations. Choosing this latter value of α gave skill scores and values of r^2 that were only slightly smaller than were obtained with the variable ν_t. This may reflect the fact that in many cases, much of the variability

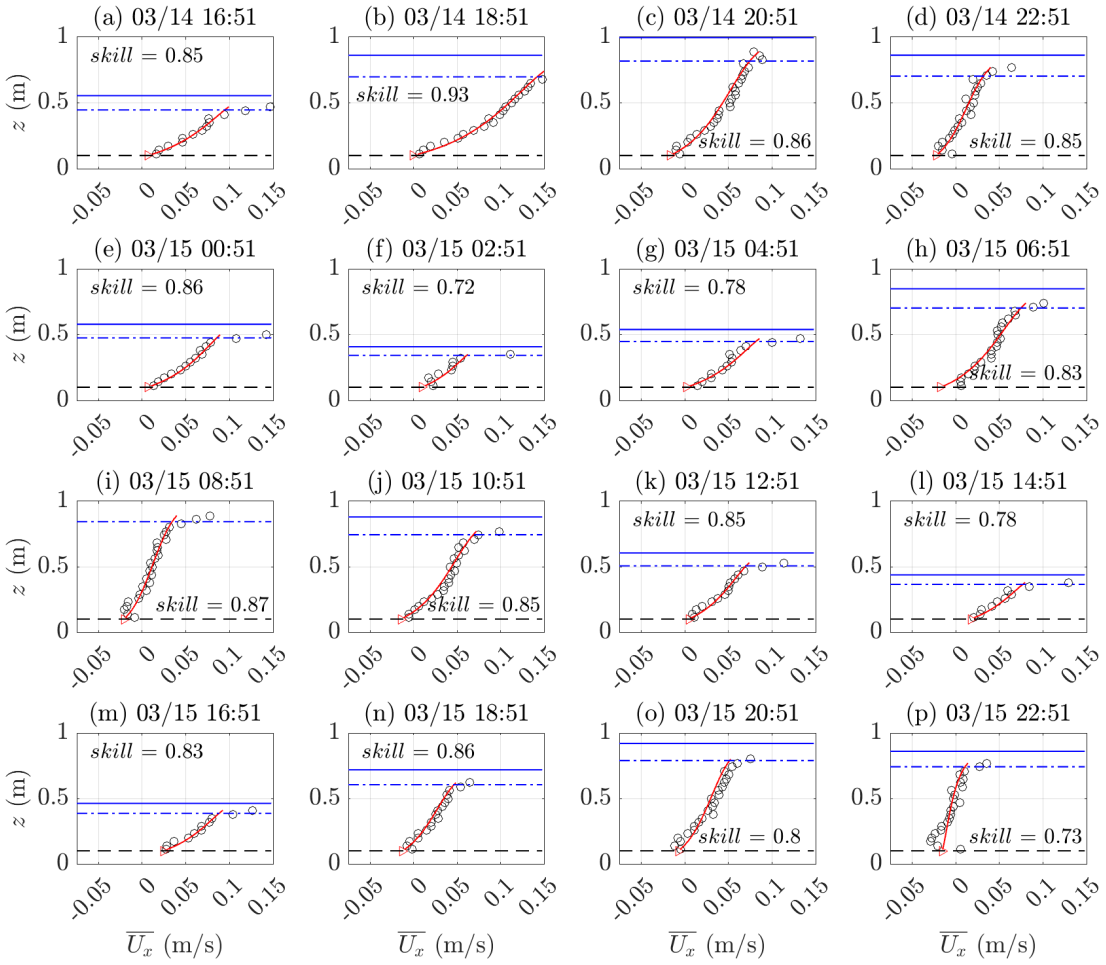

Figure 4: Comparison of predicted and observed flows on the Ofu reef flat for a period when the mean Eulerian flow is generally onshore. Times and the associated value of r^2 for the fit of the model to observations are shown for each profile. The symbols are as follows: Observations (∘); Water surface at $z = h_i$ (—); Wave trough at $z = h_i - H_s/2$ (– –); $z = z_b$ (– –); Model(—); U_0 (▷). The median model skill for this set of profiles is 0.85.

in $\overline{U}_x$ takes place near the reef surface and free surface, places where ν_t is expected to be somewhat smaller than its average value. Thus, in the absence of measurements of turbulent stresses, or of detailed velocity measurements near the bottom boundary, where the effects of variations in ν_t might be most pronounced, both models for ν_t might be viewed as equally appropriate.

Lastly, the Achilles heel of the model presented here is the need to specify U_0. The mean flow model presented here properly predicts the variation of velocity in the water column and how that variation depends on the forcing. But what the model doesn't provide is a prediction for U_0. One surprising result is that it appears that U_0 is not a function of $< \overline{U}_x >$ (Fig. 8a): a linear regression of U_0 as a function of $< \overline{U}_x >$ has $r^2 \approx 0$. Likewise, U_0 also does not depend explicitly on h_i (not shown).

Remarkably, U_0 is almost entirely negative (offshore) and varies with wave height. The analysis of Longuet-Higgins (1953) predicts an onshore streaming velocity immediately above the wave boundary layer that in the long-wave limit is given by the expression

$$U_S = \frac{5}{4}\frac{\overline{\tilde{\eta}^2}}{h_i^2}\sqrt{g h_i} \tag{17}$$

While the direction of the flow predicted by Longuet-Higgins is opposite to what is required, the dependence of U_0 on $\overline{\tilde{\eta}^2}$ and h_i predicted by eq. 17 is similar to what is observed (Fig. 8b), although the constant of proportionality is smaller and there is a small offset. Arguably, offshore streaming is an effect of the asymmetry of the waves: As seen in computations of waves and wave-driven flows on sloping bathymetry reported by Fuhrman et al. (2009), asymmetrical waves, like the broken waves observed on the Ofu reef flat

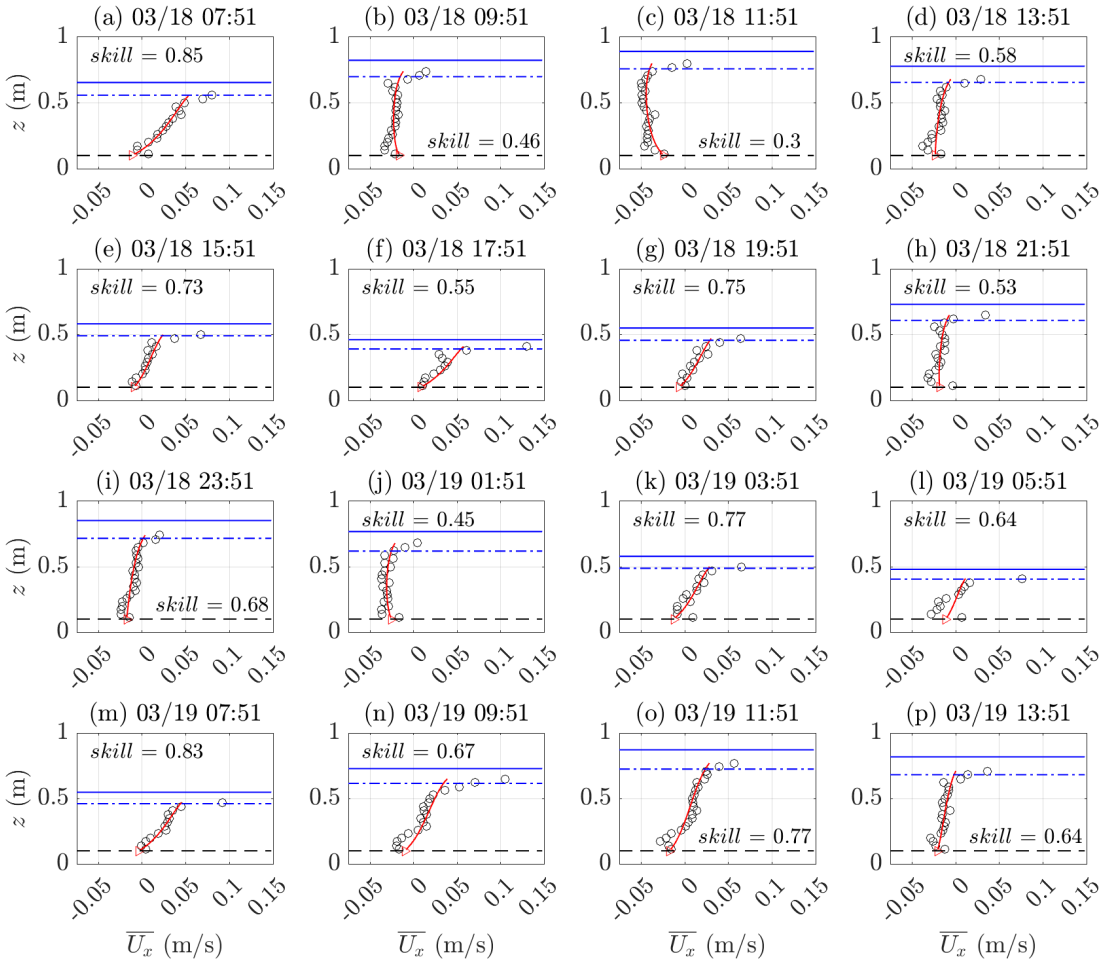

Figure 5: Comparison of predicted and observed flows on the Ofu reef flat for a period when the mean Eulerian flow often shows offshore flows (undertow) in the lower part of the water column. Times and the associated value of r^2 for the fit of the model to observations are shown for each profile. The symbols are as in 4. The median model skill for this set of profiles is 0.66.

(Maticka et al., 2022), can produce streaming flows that are directed offshore.

Although U_0 appears to be a function of $\overline{\tilde{\eta}^2}$, as are the forcing terms in eq. 7, it does not seem likely that U_0 arises from errors in computing either $\overline{\tilde{U}_x^2}$ or S_{xx} since these terms create vertical variations in the computed flow. Nonetheless, it is possible that values of U_0 we derived may have been associated with systematic errors in the values of τ_b inferred by Maticka et al. (2022) using the depth-averaged momentum balance, although this too would affect the vertical structure of predicted flows. Clearly, it would be better in the future to directly measure the bottom stress, although this would require using some form of wave-turbulence separation technique (see e.g., Davis et al. (2021)).

5. Summary and Conclusions

In this paper we have presented a model of the vertical structure of flows on reef flats inshore of where waves arriving from offshore have broken. As seen on the reef flat at Ofu, American Samoa (Maticka et al., 2022), this region appears to be similar to the surf zone on beaches in that it is a place where the broken waves tend to be bore-like and the flows tend to be highly turbulent. The nature of these flows depends on the extent to which the overall reef system appears "open", i.e., resistance to flow through the system is sufficiently small for there to be shore-ward mean flows on the reef flat (Lindhart et al., 2021). In contrast, if flow resistance is high, the system appears "closed", i.e., the net flow over the reef flat is close to zero, and the reef appears to behave like a beach where, outside of rip currents, net shore-ward flows are zero (Lindhart et al., 2021; Maticka et al., 2022).

The model we derive is based on the analysis of Svendsen (1984b), although it is practically identical to that used by Reniers et al. (2004) in that it considers the wave-averaged dynamics of the mean Eulerian flow present below the wave troughs. This formulation shows that there is a net force

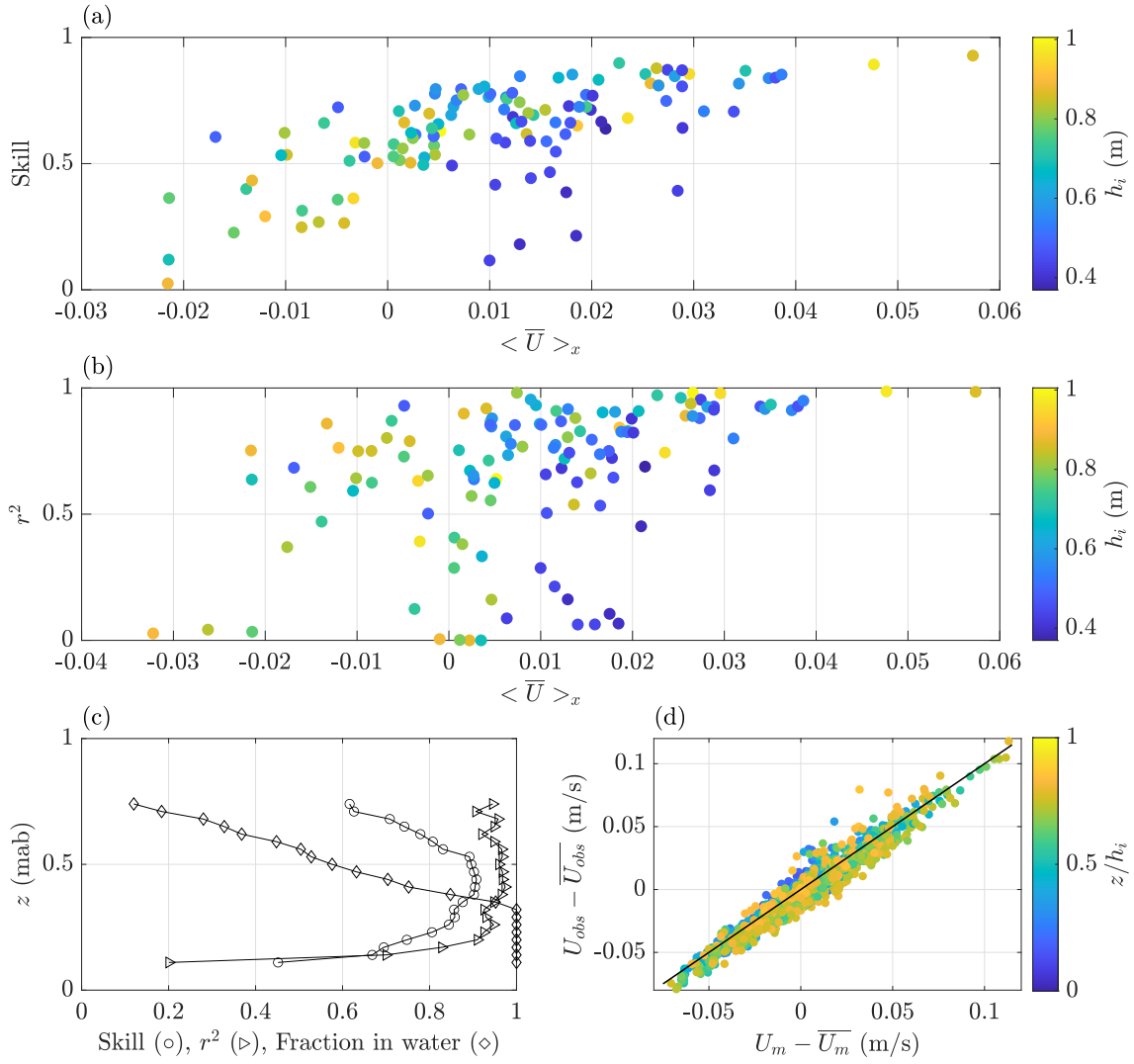

Figure 6: Variation of (a) model skill and (b) r^2 for velocity profiles computed using the parabolic viscosity model. The color of symbols indicates the mean depth. Panel c shows skill and r^2 computed for velocity time series at each depth, as well as the fraction of time each depth was in the water. Panel d shows all observed velocities as a function of computed velocities, both less their depth-averaged means. In panel d, color is used to indicate position within the water column, and the solid line indicates perfect correlation between observed and computed velocities.

present below the wave troughs even when according to the depth-averaged momentum balance, the pressure gradient balances the radiation stress gradient. As first shown by Svendsen (1984b), this net force must be balanced by a shear stress gradient, leading to the creation of "undertow", offshore flow near the bed (and possibly higher). As described by Reniers et al. (2004), the turbulent shear stress can be modeled with an eddy viscosity parameterized in terms of the local wave properties. In the present case, with the wave properties and bottom stress both known *a priori*, this analysis requires two parameters, one for scaling the eddy viscosity, α, the other the near-bed velocity, U_0.

Fitting the vertical structure model to the observations of reef flat flows made on Ofu, American Samoa and reported by Maticka et al. (2022) shows that choosing $\alpha = 0.07$ and specifying U_0 so that computed and observed depth-averaged flows leads to reasonably accurate model predictions. The quality of the model is seen in both Wilmott skill scores and values of r^2 for time series predictions at different depths that are greater than 0.9 for much of the water column. Examining the model on a profile by profile basis (rather than by time series at different depths), the model is seen to do best at high water and when flows are strongly onshore, although it does predict offshore flows, notably even at times when the overall flow is onshore. However, the near-bottom

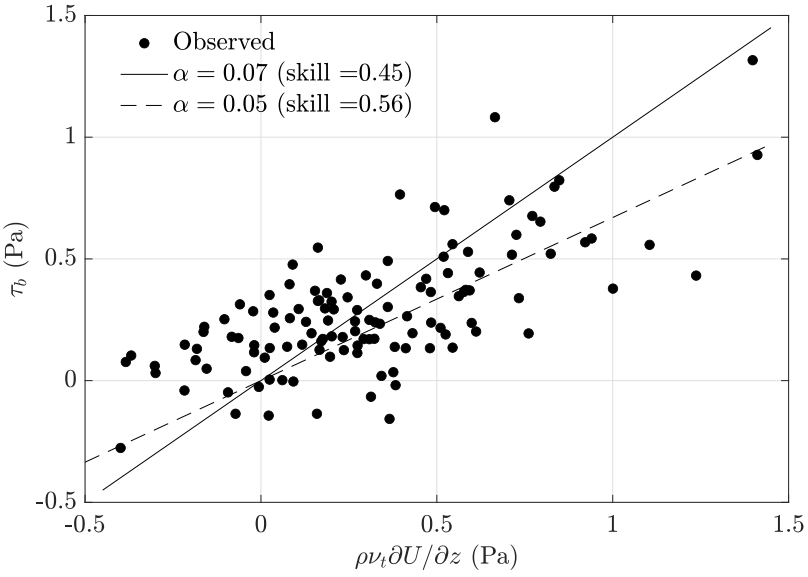

Figure 7: Modeled bottom stress and bottom stress derived from the 1D cross-reef momentum balance (Maticka et al., 2022): Modeled stress with $\alpha = 0.07$ (•); 1:1 fit of model to observations (—-); $\alpha = 0.05$ chosen to best fit model to observations (− − −)

velocity U_0 cannot be specified *a priori* and is comparable to the overall depth-averaged mean Eulerian flow. Thus, at present what the model does best is predict the shear in the water column.The source of this indeterminacy remains to be determined, although the observed dependence of U_0 on U_S suggests that U_0 is associated with boundary layer streaming.

It also would be useful to measure turbulent stresses and so improve the formulation of the eddy viscosity model, i.e., the dependence of ν_t on wave properties and on reef roughness, behavior that we did not explore. In a like fashion it would clearly be of great value to measure the velocity and turbulence near the free surface, notably to enable estimation of R or equivalently values of S_{xx} that are based on the total wave momentum flux, rather than only the momentum flux associated with a depth-uniform, long-wave velocity integrated over the wave-averaged depth.

Finally, the flows we considered in this paper are common ones on coral reefs (Péquignet et al., 2011; Storlazzi et al., 2018). Such flows can play an important role in reef bioegeochemistry and ecology, for example, by controlling mass transfer between the reef and overlying waters (Falter et al., 2013), by determining net transport or retention of larvae (Davis et al., 2021), or by dissipating low-frequency storm waves that can lead to destructive reef overtopping on atolls (Storlazzi et al., 2018). Thus, continuing to improve models of reef flat flows like that shown here seems warranted from a practical as well as a scientific perspective.

Acknowledgments

The authors are grateful for support of this work by the National Science Foundation through grants OCE-1536502, OCE-1536618, OCE-1736668, and OCE-1948189. We also thank Pago Pago Marine Charters, Annie Adelson and Emma Reid for their help with the 2017 field work, Falk Feddersen for his critical review of an earlier version of the analysis given here, and two anonymous reviewers whose suggestions provided valuable improvements to our paper. This work was conducted under permits from the U.S. Department of the Interior National Park Service, National Park of American Samoa, and the American Samoa Department of Marine and Wildlife Resources.

CRediT authorship contribution statement

Stephen G. Monismith: Study design and execution, data analysis, manuscript preparation. **Samantha A. Maticka:** Study design and execution, data analysis, manuscript preparation. **Justin S. Rogers:** Study design and execution. **Ben Hefner:** Study execution, data analysis. **C. Brock Woodson:** Study design and execution, data analysis, manuscript preparation.

References

Apotsos, A., Raubenheimer, B., Elgar, S., Guza, R.T., 2008. Wave-driven setup and alongshore flows observed onshore of a submarine canyon. Journal of Geophysical Research: Oceans 113. URL: https://agupubs.onlinelibrary.wiley.com/doi/abs/10.1029/2007JC004514, doi:https://doi.org/10.1029/2007JC004514.

Apotsos, A., Raubenheimer, B., Elgar, S., Guza, R.T., Smith, J.A., 2007. Effects of wave rollers and bottom stress on wave setup. Journal of Geophysical Research: Oceans 112. URL: https://agupubs.onlinelibrary.wiley.com/doi/abs/10.1029/2006JC003549, doi:https://doi.org/10.1029/2006JC003549.

Battjes, J.A., 1988. Surf-zone dynamics. Annual Review of Fluid Mechanics 20, 257–291. doi:10.1146/annurev.fl.20.010188.001353.

Becker, J.M., Merrifield, M.A., Ford, M., 2014. Water level effects on breaking wave setup for Pacific island fringing reefs. Journal of Geophysical Research: Oceans 119, 914–932. URL: https://agupubs.onlinelibrary.

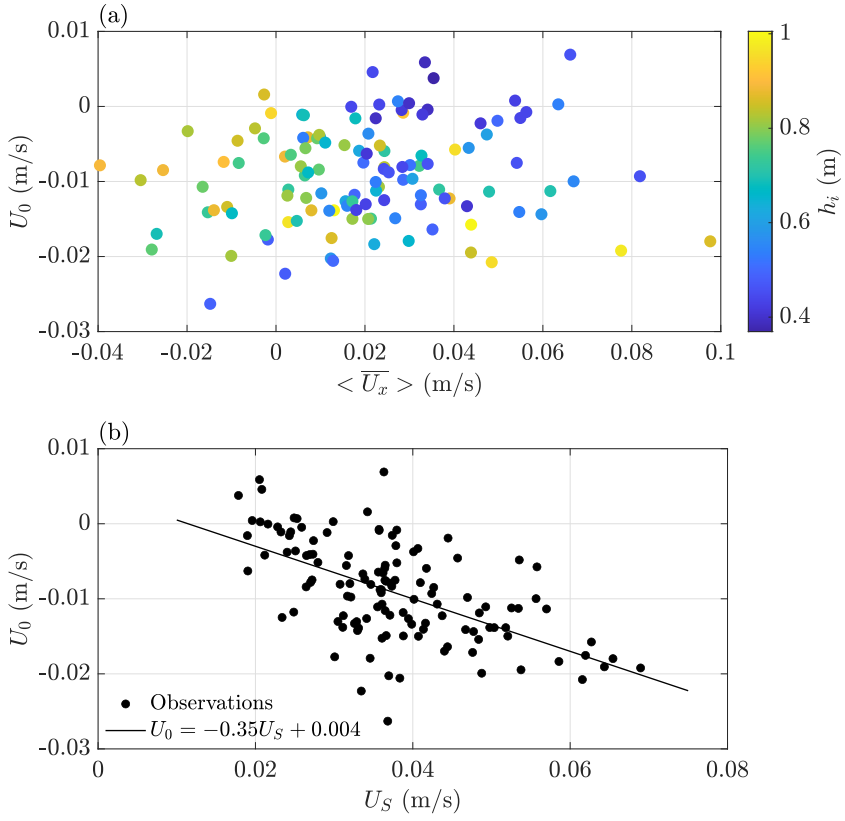

Figure 8: (a) U_0 as a function of the depth-average mean Eulerian velocity $< \overline{U_x} >$. Here, the color of the symbols shows the mean depth for each profile. (b) U_0 as a function of the boundary layer streaming velocity (eq. 17). The solid line in b is the least squares fit to the data ($r^2 = 0.33$).

wiley.com/doi/abs/10.1002/2013JC009373, doi:https://doi.org/10.1002/2013JC009373.

Buckley, M.L., Lowe, R.J., Hansen, J.E., Dongeren, A.R.V., 2015. Dynamics of wave setup over a steeply sloping fringing reef. Journal of Physical Oceanography 45, 3005 – 3023.

Buckley, M.L., Lowe, R.J., Hansen, J.E., Dongeren, A.R.V., 2016. Wave setup over a fringing reef with large bottom roughness. Journal of Physical Oceanography 46, 2317 – 2333. URL: https://journals.ametsoc.org/view/journals/phoc/46/8/jpo-d-15-0148.1.xml, doi:10.1175/JPO-D-15-0148.1.

Davis, K.A., Pawlak, G., Monismith, S.G., 2021. Turbulence and coral reefs. Annual Review of Marine Science 13, 343–373. doi:10.1146/annurev-marine-042120-071823. pMID: 32762591.

Falter, J.L., Lowe, R.J., Zhang, Z., McCulloch, M., 2013. Physical and biological controls on the carbonate chemistry of coral reef waters: effects of metabolism, wave forcing, sea level, and geomorphology. PLoS One 8, e53303.

Fuhrman, D.R., Fredsøe, J., Sumer, B.M., 2009. Bed slope effects on turbulent wave boundary layers: 2. comparison with skewness, asymmetry, and other effects. Journal of Geophysical Research: Oceans 114. doi:https://doi.org/10.1029/2008JC005053.

Govender, K., Michallet, H., Alport, M., 2011. Dciv measurements of flow fields and turbulence in waves breaking over a bar. European Journal of Mechanics - B/Fluids 30, 616–623.

Grant, S.B., Kim, J.H., Jones, B.H., Jenkins, S.A., Wasyl, J., Cudaback, C., 2005. Surf zone entrainment, along-shore transport, and human health implications of pollution from tidal outlets. Journal of Geophysical Research: Oceans 110. URL: https://agupubs.onlinelibrary.wiley.com/doi/abs/10.1029/2004JC002401, doi:https://doi.org/10.1029/2004JC002401.

Hefner, Ben B.and Rogers, J.S., Maticka, S.A., Monismith, S.G., Woodson, C.B., 2019. Instrumentation for direct measurements of wave-driven flow over a fringing reef crest. Limnology and Oceanography: Methods 17, 627–638. doi:doi:10.1002/lom3.10337.

Lindhart, M., Rogers, J.S., Maticka, S.A., Woodson, C.B., Monismith, S.G., 2021. Wave modulation of flows on open and closed reefs. Journal of Geophysical Research: Oceans 126, e2020JC016645. doi:https://doi.org/10.1029/2020JC016645.

Longuet-Higgins, M., 1969. On the transport of mass by time-varying ocean currents. Deep Sea Research and Oceanographic Abstracts 16, 431–447. URL: https://doi.org/10.1016/0011-7471(69)90031-X.

Longuet-Higgins, M., 2005. On wave set-up in shoaling water with a rough sea bed. Journal of Fluid Mechanics 527, 217–234. doi:10.1017/S0022112004003222.

Longuet-Higgins, M., Stewart, R.W., 1962. Radiation stress and mass transport in gravity waves, with application to 'surf beats'. Journal of Fluid Mechanics 13, 481–504. doi:10.1017/S0022112062000877.

Longuet-Higgins, M.S., 1953. Mass transport in water waves. Philosophical Transactions of the Royal Society of London. Series A, Mathematical and Physical Sciences 245, 535–581. doi:10.1098/rsta.1953.0006.

Lowe, R.J., Falter, J.L., Bandet, M.D., Pawlak, G., Atkinson, M.J., Monismith, S.G., Koseff, J.R., 2005. Spectral wave dissipation over a barrier reef. Journal of Geophysical Research: Oceans 110.

Martins, K., Blenkinsopp, C.E., Deigaard, R., Power, H.E., 2018. Energy dissipation in the inner surf zone: New insights from lidar-based roller geometry measurements. Journal of Geophysical Research: Oceans 123, 3386–3407. URL: https://agupubs.onlinelibrary.wiley.com/doi/abs/10.1029/2017JC013369, doi:https://doi.org/10.1029/2017JC013369.

Maticka, S.A., 2019. A tale of two reefs: Hydrodynamics of a fringing reef and a reef atoll. Ph.D. thesis. Stanford University.

Maticka, S.A., Rogers, J.S., Woodson, C.B., Hefner, B.B., Monismith, S.G., 2022. Reef flat flow dynamics for a nearly closed fringing reef lagoon: Ofu, american samoa. Journal of Geophysical Research: Oceans 127, e2022JC018831. doi:https://doi.org/10.1029/2022JC018831.

Mei, C.C., Stiassnie, M., Yue, D.K.P., 1989. Theory and Applications of Ocean Surface Waves: Part 1: Linear Aspects Part 2: Nonlinear Aspects. World Scientific.

Monismith, S.G., 2014. Flow through a rough, shallow reef. Coral Reefs 33, 99–104.

Monismith, S.G., Herdman, L.M., Ahmerkamp, S., Hench, J.L., 2013. Wave transformation and wave-driven flow across a steep coral reef. Journal of Physical Oceanography 43, 1356–1379.

Monismith, S.G., Rogers, J.S., Koweek, D., Dunbar, R.B., 2015. Frictional wave dissipation on a remarkably rough reef. Geophysical Research Letters 42, 4063–4071.

Morgan, S.G., Shanks, A.L., MacMahan, J.H., Reniers, A.J., Feddersen, F., 2018. Planktonic subsidies to surf-zone and intertidal communities. Annual Review of Marine Science 10, 345–369. doi:10.1146/annurev-marine-010816-060514. pMID: 28846492.

Nielsen, P., 1992. Coastal bottom boundary layers and sediment transport. volume 4. World Scientific Publishing Company.

Oliver, T.A., Palumbi, S.R., 2009. Distributions of stress-resistant coral symbionts match environmental patterns at local but not regional scales. Marine ecology progress series 378, 93–103.

Péquignet, A.C.N., Becker, J.M., Merrifield, M.A., Boc, S., 2011. The dissipation of wind wave energy across a fringing reef at Ipan, Guam. Coral Reefs 30, 71–82.

Pope, S.B., 2000. Turbulent Flows. Cambridge University Press.

Raubenheimer, B., Guza, R.T., Elgar, S., 1996. Wave transformation across the inner surf zone. Journal of Geophysical Research: Oceans 101, 25589–25597.

Raubenheimer, B., Guza, R.T., Elgar, S., Kobayashi, N., 1995. Swash on a gently sloping beach. Journal of Geophysical Research: Oceans 100, 8751–8760. doi:https://doi.org/10.1029/95JC00232.

Reniers, A.J.H.M., Thornton, E.B., Stanton, T., Roelvink, D., 2004. Vertical flow structure during Sandy Duck: observations and modeling. Coastal Engineering 51, 237–260. URL: https://www.sciencedirect.com/science/article/pii/S0378383904000171, doi:https://doi.org/10.1016/j.coastaleng.2004.02.001.

Roelvink, D., Reniers, A.J.H.M., 2012. A guide to modeling coastal morphology. volume 12. Singapore.

Rogers, J.S., Maticka, S.A., Chirayath, V., Woodson, C.B., Alonso, J.J., Monismith, S.G., 2018. Connecting flow over complex terrain to hydrodynamic roughness on a coral reef. Journal of Physical Oceanography 48. doi:https://doi.org/10.1175/JPO-D-18-0013.1.

Ruessink, B.G., Miles, J.R., Feddersen, F., Guza, R.T., Elgar, S., 2001. Modeling the alongshore current on barred beaches. Journal of Geophysical Research: Oceans 106, 22451–22463. URL: https://agupubs.onlinelibrary.wiley.com/doi/abs/10.1029/2000JC000766, doi:https://doi.org/10.1029/2000JC000766.

Sous, D., Maticka, S., Meulé, S., Bouchette, F., 2022. Bottom drag coefficient on a shallow barrier reef. Geophysical Research Letters 49, e2021GL097628. URL: https://agupubs.onlinelibrary.wiley.com/doi/abs/10.1029/2021GL097628, doi:https://doi.org/10.1029/2021GL097628.

Stive, M., Wind, H., 1982. A study of radiation stress and set-up in the nearshore region. Coastal Engineering 6, 1–25. doi:https://doi.org/10.1016/0378-3839(82)90012-6.

Storlazzi, C.D., Gingerich, S.B., van Dongeren, A., Cheriton, O.M., Swarzenski, P.W., Quataert, E., Voss, C.I., Field, D.W., Annamalai, H., Piniak, G.A., et al., 2018. Most atolls will be uninhabitable by the mid-21st century because of sea-level rise exacerbating wave-driven flooding. Science advances 4, eaap9741.

Svendsen, I., 1984a. Wave heights and set-up in a surf zone. Coastal Engineering 8, 303–329. URL: https://www.sciencedirect.com/science/article/pii/0378383984900280, doi:https://doi.org/10.1016/0378-3839(84)90028-0.

Svendsen, I.A., 1984b. Mass flux and undertow in a surf zone. Coastal Engineering 8, 347–365.

Symonds, G., Black, K.P., Young, I.R., 1995. Wave-driven flow over shallow reefs. Journal of Geophysical Research: Oceans 100, 2639–2648.

Thornton, E.B., Guza, R.T., 1983. Transformation of wave height distribution. Journal of Geophysical Research: Oceans 88, 5925–5938.

Willmott, C.J., 1981. On the validation of models. Physical Geography 2, 184–194. doi:10.1080/02723646.1981.10642213.

Yao, Y., Huang, Z., Monismith, S.G., Lo, E.Y., 2012. 1DH Boussinesq modeling of wave transformation over fringing reefs. Ocean Engineering 47, 30–42. doi:https://doi.org/10.1016/j.oceaneng.2012.03.010.